Uniform biodegradable fiber-like micelles and block comicelles via "living" crystallization-driven self-assembly of poly($_L$-lactide) block copolymers

He, Yunxiang; Eloi, Jean-Charles; Harniman, Robert L ; Richardson, Robert M.; Whittell, George R; Mathers, Robert T.; Dove, Andrew; O'Reilly, Rachel; Manners, Ian

Link to publication on Research at Birmingham portal

Uniform Biodegradable Fiber-Like Micelles and Block Co-micelles via 'Living' Crystallization-Driven Self-Assembly of Poly(*L*-lactide) Block Copolymers: The Importance of Reducing Unimer Self-Nucleation via Hydrogen Bond Disruption

Yunxiang He,[1] Jean-Charles Eloi,[1] Robert L. Harniman,[1] Robert M. Richardson,[2] George R. Whittell,[1] Robert T. Mathers,[3] Andrew P. Dove,[4*] Rachel K. O'Reilly,[4*] and Ian Manners[1,5*]

[1]School of Chemistry, University of Bristol, Bristol BS8 1TS, UK

[2]School of Physics, University of Bristol, Tyndall Avenue, Bristol, BS8 1TL, UK

[3]Department of Chemistry, Pennsylvania State University, New Kensington, PA 15068, USA

[4]School of Chemistry, University of Birmingham, Edgbaston, Birmingham, B15 2TT, UK

[5]Department of Chemistry, University of Victoria, Victoria, BC V8W 3V6, Canada

[*]To whom correspondence should be addressed:

a.dove@bham.ac.uk

r.oreilly@bham.ac.uk

imanners@uvic.ca

ABSTRACT

Fiber-like micelles based on biodegradable and biocompatible polymers exhibit considerable promise for applications in nanomedicine, but until recently no convenient methods were available to prepare samples with uniform and controllable dimensions and spatial control of functionality. 'Living' crystallization-driven self-assembly (CDSA) is a seeded growth method of growing importance for the preparation of uniform 1D and 2D core-shell nanoparticles from a range of crystallizable polymeric amphiphiles. However, in the case of poly(*L*-lactide) (PLLA), arguably the most widely utilized biodegradable polymer as the crystallizable core-forming block, the controlled formation of uniform fiber-like structures over a substantial range of lengths by 'living' CDSA has been a major challenge. Herein, we demonstrate that via simple modulation of the solvent conditions via the addition of trifluoroethanol (TFE), DMSO, DMF and acetone, uniform fiber-like nanoparticles from PLLA diblock copolymers with controlled lengths up to 1 μm can be prepared. The probable mechanism involves improved unimer solvation by a reduction of hydrogen bonding interactions among PLLA chains. We provide evidence that this minimizes undesirable

unimer aggregation which otherwise favors self-nucleation that competes with epitaxial crystallization from seed termini. This approach has also allowed the formation of well-defined segmented block co-micelles with PLLA cores via the sequential seeded-growth of PLLA block copolymers with different corona-forming blocks.

INTRODUCTION

The solution self-assembly of amphiphilic block copolymers (BCPs) with amorphous core-forming blocks has been widely studied as a method for fabricating nanoparticles with morphologies such as spheres, cylinders/worms or 'fiber-like' micelles, platelets and vesicles.[1-4] Cylinders or fiber-like micelles are attracting much interest particularly in biomedicine, due to the advantages of extended *in vivo* circulation times and improved cellular uptake behavior that have been observed in several comparative studies with spherical particles.[5-8] However, morphologically pure samples of fiber-like micelles with amorphous core-forming blocks are challenge to access by BCP self-assembly as they generally correspond to a restricted region of phase space.[9-11] Furthermore, access to low dispersity samples of controlled length has not been possible.[12-18]

Recent work has demonstrated that BCPs and related amphiphiles with a crystalline core-forming block readily form 1D fibers via a process termed crystallization-driven self-assembly (CDSA).[10-11, 19] Moreover, seeded-growth methods have been developed which allow length control and access to low length dispersity samples. This process shows many analogies with living covalent polymerizations and has been termed 'living CDSA' (Scheme 1).[20-22] In the most common form of living CDSA, polydisperse fiber-like micelles are prepared first in solution and are then fragmented by sonication to form small fragments or 'seeds'. The termini of the seeds are active to epitaxial growth of the additional BCP. Furthermore, adjustment of the ratio of the added BCP to the seeds, yields fiber-like micelles of controlled length and a low length dispersity.
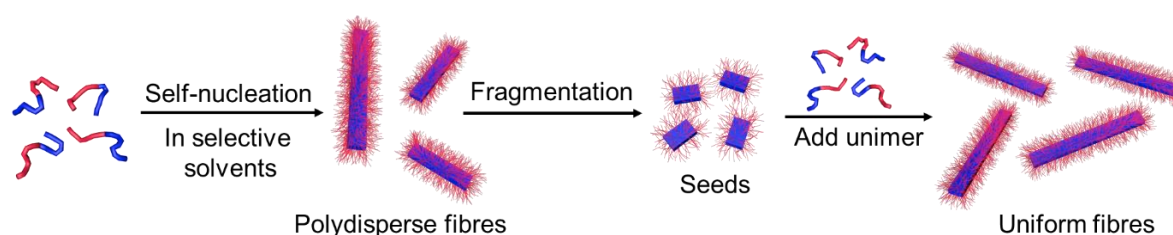
Scheme 1. Schematic representation of uniform fibers prepared by seeded-growth method of living CDSA.

The living CDSA method was initially developed using BCPs with crystallizable poly(ferrocenyldimethylsilane) (PFS)[23] core-forming block. Cylinders can be formed with a wide range of corona-core block ratios from ca. 6:1 to 22:1,[24-25] and using living CDSA can be prepared with lengths controlled from ca. 20 nm to > 5 μm.[21, 26] The sequential addition of PFS BCPs with different corona-forming blocks yields segmented block co-micelles.[27] The formation of 1D block co-micelles that possess spatially-defined coronal regions with complementary hydrogen-bonding (H-bonding) groups allows access to supermicelles via hierarchical self-assembly.[28] In addition, 2D platelets with controlled size have been prepared from diblock copolymers with low corona-core block ratios,[29] blends of diblock copolymers and homopolymer,[30] and charge-terminated homopolymers.[31] The properties and applications of PFS-based micelles and supermicelles have also been explored, including their lyotropic liquid crystalline phase behavior,[32] use in surface patterning,[33] dispersion in aqueous media[34] and subsequent use in interface stabilization to form colloidosomes.[35]

Studies on fiber-like micelle formation with BCPs with a crystallizable core-forming block have been extended to other materials, such as polyethylene[36-39] and π-conjugated polymers.[40-53] In order to develop applications in nanomedicine, well-defined 1D micelles based on crystalline biodegradable and biocompatible polymers are highly desirable. Poly(*L*-lactide) (PLLA), poly(ε-caprolactone) (PCL) and polycarbonates fulfill these requirements and possess a trend in their ease of biodegradation (PLLA > PCL > polycarbonates).[54-55] Exploration of living CDSA approaches to yield well-defined 1D and 2D assemblies derived from these materials as core-forming blocks has attracted much attention.[56-70] Examples of length control of up to ca. 800 nm have been described for PCL-containing fibers in ethanol. After transferring seeds into water by dialysis, living CDSA was successfully performed directly in aqueous media.[71] In addition, a recent report[72] described the successful extension of seeded-growth methods to polycarbonate-based fiber-like micelles.

In contrast, the efficient use of living CDSA methods for PLLA BCPs has been a substantial challenge. Initial studies in 2011 demonstrated that fine-tuning the self-assembly solvent composition and temperature allowed the formation of uniform micelles with length up to 300 nm.[56, 58] By altering the solvation of the PLLA core-forming block, transitions between spheres (with kinetically-trapped amorphous cores) and cylinders (with crystalline cores) have been studied.[57] Further work revealed a remarkable reverse morphology change from cylinders to spheres triggered by the stereocomplexation of two enantiomeric BCPs with PLLA and poly(*D*-lactide) (PDLA) core-forming blocks.[63] More recently, the solubility of

PLLA-containing diblock copolymers has been found to have another interesting and unexpected effect on the morphology formation.[64] A high corona-core block ratio leads to a preference for the formation of 2D platelet micelles, while a low ratio was found to lead to 1D cylindrical micelles. This behavior is the opposite to that usually observed for self-assembled BCPs with crystallizable core-forming blocks and contrasts with that predicted by packing-parameter considerations. In other studies spherical, cylindrical, and platelet-like micelles have been reported for block copolymers with PLLA cores and glucose carbonate coronas.[73] In addition, the CDSA of PLLA-based diblock and triblock copolymers has also been characterized in detail by establishment of a phase diagram mapping the morphology formed versus hydrophobic fraction.[65] Significantly, uniform 2D platelets with PLLA cores can be obtained under thermal self-seeding conditions in which seed formation is controlled by temperature.[74] In another study, 2D platelets with controlled dimensions and block co-platelets spatially segmented structures have been reported using seeded-growth of a charge-terminated PLLA homopolymers.[31, 75] However, no uniform 1D fiber-like micelles of PLLA-based diblock copolymers with length control over a wide range have been reported via a seeded-growth process under mild conditions.

Herein, we discuss the results of a detailed collaborative exploration of the 'living' CDSA of PLLA-containing diblock copolymers in an attempt to improve the length control of PLLA fiber-like micelles. This has led to the development of a new approach involving the addition of solvents which minimize unimer self-nucleation and thereby allow access to low dispersity samples of controlled length over a substantial length range. We have also applied the new method to prepare previously unknown PLLA-based block co-micelles with a segmented coronal architecture.

RESULTS

1. PLLA BCP Synthesis and Characterization.

In this work, we have focused our studies on two PLLA BCPs, PLLA-*b*-Poly(N-isopropylacrylamide) (PLLA-*b*-PNIPAm) and PLLA-*b*-Poly(2-vinylpyridine) (PLLA-*b*-P2VP) (Figure 1). In order to favor 1D fiber-like micelles formation, block ratios were targeted in which the degree of polymerization (DP_n) of the corona-forming block was substantially larger than that of PLLA segment. The diblock copolymers were prepared by a combination of ring-opening polymerization (ROP) and a Reversible Addition−Fragmentation Transfer (RAFT) polymerization (Scheme S1). The polymer molar

mass characteristics were analyzed by various technique (Figure S1-S3 and Table S1). To confirm the purity of the diblock copolymer, DOSY NMR spectroscopic analysis was employed to complement GPC characterization. In the DOSY spectra of the $PLLA_{47}$-b-$PNIPAm_{267}$ and $PLLA_{47}$-b-$P2VP_{503}$ (Figure S4), all the signals appeared at the same position in each spectrum and with a diffusion coefficient of $D = 1.31 \times 10^{-6}$ and 7.26×10^{-6} $cm^2 \cdot s^{-1}$, respectively, which indicated successful preparation of essentially pure diblock copolymers devoid of homopolymer impurities.
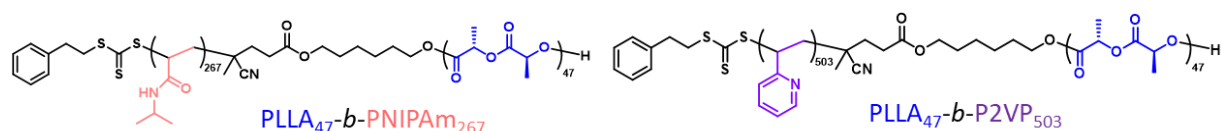
Figure 1. Structures of $PLLA_{47}$-b-$PNIPAm_{267}$ and $PLLA_{47}$-b-$P2VP_{503}$.

The prepared polymers were also characterized by Fourier-transform infrared spectroscopy (FT-IR) (Figure S5) and thermogravimetric analysis (TGA) was carried out on the diblock copolymers (Figure S6). The latter showed that the decomposition temperatures (defined as the temperatures of 5% mass loss) of $PLLA_{47}$-b-$PNIPAm_{267}$ and $PLLA_{47}$-b-$P2VP_{503}$ were determined to be 245 and 295 °C, respectively.

2. Fiber-Like Micelle Formation and Seed Micelle Preparation

Fiber-like micelles of PLLA-b-PNIPAm was prepared by the direct dissolution method according to previous reported procedures.[20, 22, 76] $PLLA_{47}$-b-$PNIPAm_{267}$ was dissolved in DMSO/EtOH (v:v = 1:9) at 70 °C for 2 h followed by slow cooling to 23 °C over 2.5 h (Figure S7a). DMSO was used as a common solvent in the self-assembly to prepare unimer solution. Although the solubility parameters for the polymer and solvent are significantly different ($\delta_{PLLA} = 20.2$ $MPa^{1/2}$, $\delta_{DMSO} = 26.4$ $MPa^{1/2}$), the formation of molecularly dissolved unimers and the absence of detectable aggregates was demonstrated by dynamic light scattering (DLS, Figure S19). EtOH was used as the selective solvent for self-assembly due to the similar solubility parameters of PNIPAm and EtOH ($\delta_{PNIPAm} = 24.8$ $MPa^{1/2}$ and δ_{EtOH} =26.2 $MPa^{1/2}$). Seed micelles were prepared by sonication of the polydisperse $PLLA_{47}$-b-$PNIPAm_{267}$ micelle solution in an ultrasonic cleaning bath for 2 h at 0 °C (Figure S7b). The prepared seed micelles had a measured number average length (L_n) of 36 nm, and a length dispersity (L_w/L_n) of 1.10 (Figure S7c).

3. Living CDSA in EtOH: Evidence for Competition between Self-nucleation and Epitaxial Growth

Elongated micelles were obtained by adding various amount of unimers (PLLA$_{47}$-b-PNIPAm$_{267}$ in DMSO) to the seed solutions in EtOH. After aging for 5 days, samples were analyzed by TEM. The images (Figure S8a-f) showed presence of small non-spherical particles in addition to the anticipated elongated fiber-like micelles. The fibers had measured L_n values from ca. 100 - 800 nm, with $L_w/L_n \geq 1.06$ depending on the unimer-to-seed mass ratios ($m_{unimer}:m_{seed}$). The lengths of elongated micelles were found to be significantly shorter than predicted values (Figure S8g). The predicted average length can be calculated from $L_n = (m_{unimer}/m_{seed} + 1) \times L_{n\ seed}$. Furthermore, the micelle length dispersity L_w/L_n and standard deviation increased significantly (from 1.06 to 1.15) with the increase of added unimer (Figure S8g).

In the contour length histograms an appreciable fraction of short fiber-like micelles was apparent with an L_n value much lower than that predicted. (Figure S9). Significantly, the shortest micelle lengths measured in each sample were longer than the average length of the seeds (36 nm). This suggests that the most likely rationale for the uncontrolled epitaxial growth is that the self-nucleation of added unimers leading to the new seeds formation and excludes the seed defects as an explanation. The formation of a very small but significant quantity of non-spherical nanoparticles (Figure S8) provides evidence that unimer aggregation can also occur sufficiently rapidly to form aggregates where the PLLA core has insufficient time to fully crystallize. This process would also deplete the reservoir of unimer available for seeded-growth.

4. Living CDSA studies for PLLA$_{47}$-b-PNIPAm$_{267}$ in EtOH in the presence of trifluoroethanol (TFE) as a H-bond disruptor

For living CDSA to be efficient, all or virtually all the added unimer needs to grow from the seed micelle termini. In the case of PLLA$_{47}$-b-PNIPAm$_{267}$, evidence for undesirable unimer aggregation to lead to self-nucleation was detected. We considered as a possible explanation for the facile unimer aggregation the formation of C−H⋯O hydrogen bonds (H-bonds) between the protons of a methyl group and the carbonyl oxygen on another polymer chain.

A crystal unit model of PLLA was constructed based on the data reported by Kanamoto[77] (Figure S10). The distance between the proton of methyl group and the oxygen atom of a carbonyl group on adjacent chain was measured. The average length is 3.4 Å, which is in the

range expected for weak H-bond formation. The C−H···O bond is an example of a weak interaction which has been probed by computational calculations[78-79] and experimentally by FT-IR spectroscopy.[80-81] The bond energy associated with a C−H···O interaction has been calculated as 4.2 − 8.4 kJ/mol, significantly smaller than that of the well-known N−H···O or O−H···O hydrogen bonds (16 − 21 kJ/mol). The weak C−H···O bond has been found to be important in the structural conformation of small molecules, nucleic acids, proteins and carbohydrates.[82-85] Based on these considerations it is therefore plausible that H-bonding plays an important role in both PLLA BCP unimer aggregation which can result in self-nucleation and the formation of non-spherical aggregates. This led us to explore the use of additives to the self-assembly solution to mitigate this potential problem.

To prevent the fast self-nucleation when adding the unimer to seed solutions, trifluoroethanol (TFE), a reagent often used as a H-bond disruption agent,[86] was added into the solvent system. The amount of added TFE was increased in line with the increase of the unimer-to-seed mass ratio. Unimer in unimer-to-seed mass ratios of 2.5, 5.0, 10.0, 15.0, 20.0, and 30.0 was added to seed solutions in TFE/EtOH with volume ratios of 3:97, 3:97, 5:95, 8:92, 10:90 and 15:85, respectively. After aging for 5 days, the samples were analyzed by TEM (Figure 2a-d). In contrast to the seeded-growth experiments performed in the absence of TFE, the measured micelle lengths possessed L_n values of up to 1103 nm, close to the predicted values, with low dispersity ($L_w/L_n \leq 1.06$) even at high unimer-to-seed mass ratios. A linear plot of the measured length versus the unimer-to-seed mass ratio was obtained (Figure 2f) with data points located on the predicted line indicative of the controlled epitaxial growth of PLLA$_{47}$-*b*-PNIPAm$_{267}$ micelles by living CDSA. Significantly, the micelle contour length histograms showed narrow distributions for each sample with different unimer-to-seed mass ratios (Figure 2e). No overlapping peaks at low L_n values were detected, consistent with the absence (or virtual absence) of self-nucleation events (Figure S11). In addition, only a very small quantity of non-spherical nanoparticles indicative of unimer aggregation were observed by TEM, in contrast to the experiments in the absence of TFE.
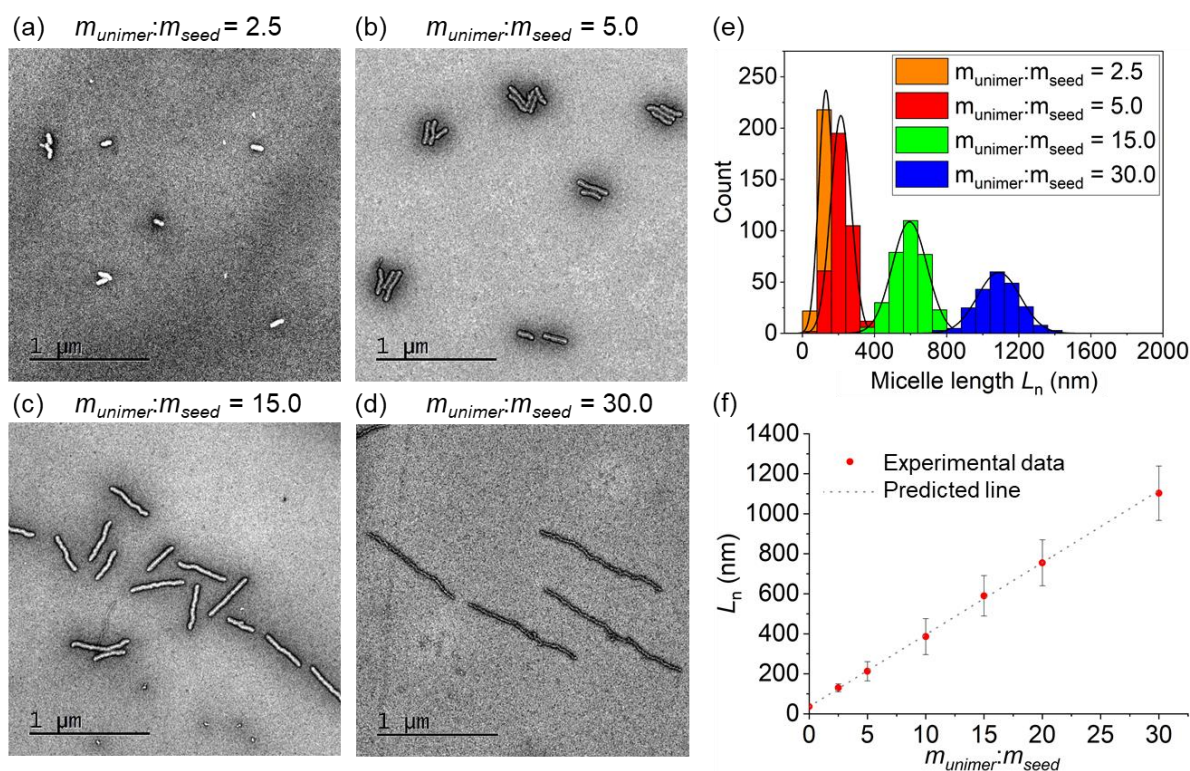
Figure 2. TEM images of samples (5 days aging) of uniform PLLA$_{47}$-*b*-PNIPAm$_{267}$ micelles prepared by seeded growth from seed micelles (L_n = 36 nm, L_w/L_n = 1.10, σ/L_n: 0.26) in TFE/EtOH with volume ratios of (a) 3:97, (b) 3:97, (c) 8:92 and (d) 15:85 after the addition of unimers (in DMSO) with unimer-to-seed mass ratios of (a) 2.5, (b) 5.0, (c) 15.0 and (d) 30.0, respectively; (e) Summary of contour length histograms of micelle length distributions; (f) plot of number average micelle length vs m_{unimer}:m_{seed} (the error bars represent the standard deviation); TEM samples were stained with a 2 wt% solution of uranyl acetate in EtOH.

5. Comparative Kinetic Studies on the Living CDSA of PLLA$_{47}$-*b*-PNIPAm$_{267}$ in the Presence and Absence of TFE

In order to explore the effect of TFE on the living CDSA growth kinetics, we studied the seeded-growth by adding PLLA$_{47}$-*b*-PNIPAm$_{267}$ unimer in DMSO to the seed solutions diluted with TFE/EtOH or pure EtOH as a control experiment over 5 days. Aliquots were taken from the solutions at set time points and were characterized by TEM after solvent evaporation. This allowed the micelle length to be monitored throughout (Figure S12-S16, Table S2 and S3).

The results (Figure 3) reveal qualitatively similar plots to those recently established in studies of the 1D growth kinetics for the living CDSA of PFS BCPs.[87] The micelles prepared in TFE/EtOH possess lengths longer than those prepared in pure EtOH at all of the set time

8

points, even after 5 days. This provided additional evidence for the reduction in self-nucleation on addition of TFE. Furthermore, the formation of small non-spherical aggregates was only detected in the absence of TFE, as noted earlier (Figure S12 vs S14) and similarly self-nucleation was evidenced by the presence of shoulder peaks in the short length range in contour length histograms (Figure S13). In the samples prepared in TFE/EtOH, no evidence for significant self-nucleation was detected (Figure S15).
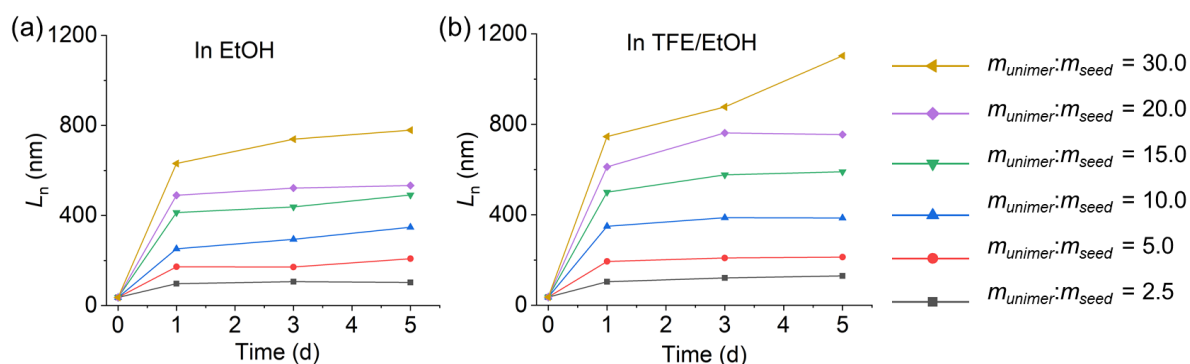
Figure 3. Kinetic studies on seeded growth of PLLA$_{47}$-b-PNIPAm$_{267}$ unimers (in DMSO) from seed micelles (0.5 mg/mL in EtOH, L_n = 36 nm, L_w/L_n = 1.10) in (a) EtOH and in (b) TFE/EtOH (v:v = 3:97, 3:97, 5:95, 8:92, 10:90 and 15:85 for m_{unimer}:m_{seed} = 2.5, 5.0, 10.0, 15.0, 20.0 and 30.0, respectively). The amount of DMSO in the final growth solutions varied from 0.6 – 3.0 vol. %. (a and b) Plots of micelle lengths verses unimer-to-seed mass ratios; (c and d) plots of micelle lengths as a function of time. The predicted length corresponding to a unimer-to-seed mass ratio of 30 is L_n = 1116 nm.

6. Influence of TFE and other Solvent Additives on Polymer Solubility and Solvent Polarity

The solvent polarity and therefore the polymer solubility would be expected to change upon addition of TFE as a cosolvent. To gain further understanding of the effect of cosolvent addition, a selection of different solvents was introduced as the cosolvent with EtOH in the seeded-growth of PLLA$_{47}$-b-PNIPAm$_{267}$. From the TEM images (Figure 4a-d, S17 and S18), controlled seeded-growth has been obtained with of four solvents with optimized volume fractions (5% DMSO, 5% DMF, 5% acetone and 10% TFE) after aging for 5 days. Higher volume fractions of cosolvent led to poorer length control in living CDSA experiments and this is attributed to significant micelle dissolution due to the improvement in core solubility in the solvent medium.
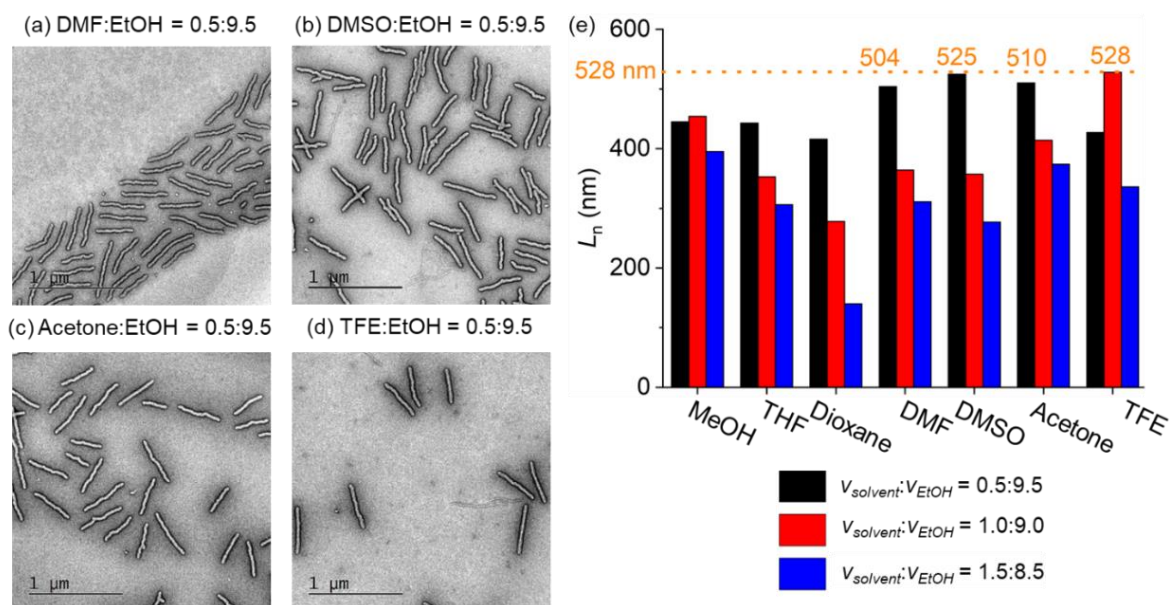
Figure 4. Seeded-growth of PLLA$_{47}$-*b*-PNIPAm$_{267}$ in different solvent mixtures after aging for 5 days: (a) in DMF:EtOH = (0.5:9.5), L_n = 504 nm; (b) in DMSO:EtOH = (0.5:9.5), L_n = 525 nm; (c) in acetone:EtOH = (0.5:9.5), L_n = 510 nm and (d) in TFE:EtOH = (1.0:9.0), L_n = 528 nm. (e) Comparison of the predicted micelle length (L_n = 528 nm) and the measured micelle length in different solvent systems.

To evaluate the change in solvent polarity and polymer solubility upon cosolvent addition, we evaluated the dielectric constant[88-90] and octanol-water partition coefficient (logP$_{oct}$) normalized by the Connolly surface area (SA). (Figure 5). LogP$_{oct}$/SA has been reported as a reliable tool with which to evaluate the hydrophobicity of polymers and solvents and to predict the most appropriate solvents for block copolymer self-assembly based on solubility.[64, 91]
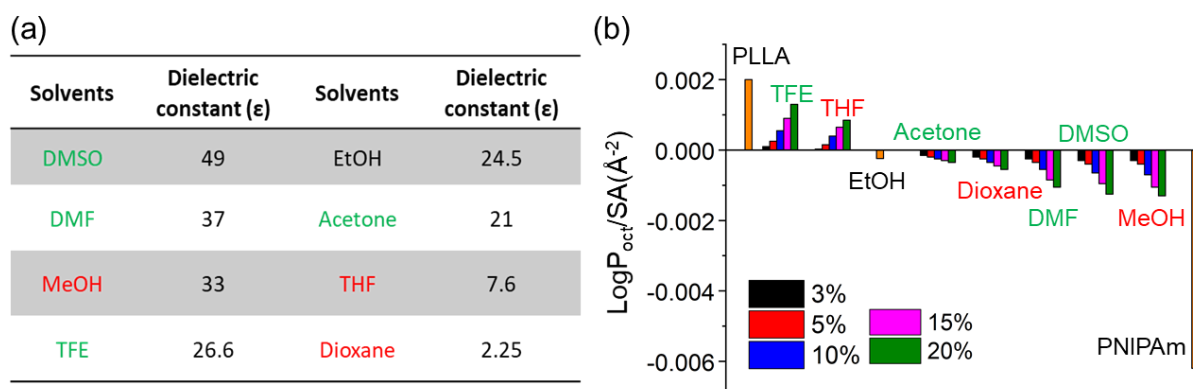
Figure 5. (a) Dielectric constants of cosolvents and (b) comparison of logP$_{oct}$/SA values between solvents and polymers. The solvents labelled in green allow controlled seeded-growth, while those

with red labels do not. Percentage values represents the volume fractions of cosolvents in the solvent system.

Comparison of the dielectric constants of selected cosolvents indicated that the polarity of solvent mixtures increased on addition of TFE, DMSO, DMF or MeOH but decreased when acetone, THF or dioxane (Figure 5a) were added. As controlled seeded-growth was observed with polar TFE, DMSO and less polar acetone and was not detected on the addition of polar MeOH, these results suggested that the solvent polarity change is not directly correlated with the observation of controlled seeded-growth.

To further study the solubility effects, first DLS was used to evaluate the dissolution of $PLLA_{47}$-b-$PNIPAm_{267}$ in different cosolvents (Figure S19). $PLLA_{47}$-b-$PNIPAm_{267}$ was present in the unimer state in all solvents except in MeOH, where aggregates with a $R_{h, app}$ value of ca. 55 nm were formed. To evaluate the polymer solubility in solvent mixtures, the calculated $logP_{oct}/SA$ values were compared (Figure 5b and S20). According to a previous report,[64] a solvent with a logP value similar to that of the corona-forming block should be an appropriate solvent for diblock copolymer self-assembly due to the promotion of the unimer solubility. However, all of the solvent mixtures studied possessed values closer to that of the core-forming block (PLLA) than to the corona-forming block (PNIPAm). This indicates that all of the solvents tested as cosolvents, even those that were found to hinder controlled living CDSA, should promote the solubility of PLLA. This would be expected to help suppress the self-nucleation to improve the seeded-growth in all cases so again no useful correlation was evident.

However, the potential disruption of PLLA intermolecular H-bonding, which would otherwise favor unimer-aggregation and self-nucleation appears to be an important factor for the controlled seeded-growth. Due to the correlations with polarity, the H-bonding capability of the cosolvents was evaluated by Dimroth and Reichardt's Transition Energy (E_T).[92-93] TFE (61.2), DMSO (44.8), DMF (43.1) and acetone (41.6) possess higher E_T values than THF (38.9) and dioxane (38.1), which indicates a stronger H-bonding capability with which to disrupt the PLLA intermolecular H-bonding (Table S4). Although MeOH has a high E_T (53.6), it precipitates PLLA to facilitate unimer aggregation and self-nucleation. Therefore, controlled seeded-growth was observed only in the presence of TFE, DMSO, DMF or acetone.

7. Structural Characterization of Uniform Fiber-Like PLLA$_{47}$-*b*-PNIPAm$_{267}$ Micelles

As living CDSA proceeds via an epitaxial growth mechanism the resulting crystalline micelle cores are highly ordered, and their structure has been likened to that of a single crystal.[31, 94-95] We therefore took advantage of living CDSA with the presence of TFE to prepare a sample of PLLA$_{47}$-*b*-PNIPAm$_{267}$ fibers with L_n = 1040 nm and L_w/L_n = 1.04 (Figure S21) to allow a detailed study of the micelle structure.

Atomic force microscopy (AFM) measurements showed that the micelles possess a uniform height of 14 nm assigned to the PLLA core (Figure 6 and S22a). The adhesion profile (Figure 6b) provided a detailed information such as the core width, and also the width of the corona flanking each side of the core predominantly lying on the substrate, giving values of 36 and 16 nm, respectively (Figure 6c). Due to the low electron density of PLLA$_{47}$-*b*-PNIPAm$_{267}$, TEM grids were negatively stained with uranyl acetate (2% in EtOH), which resulted in a difficulty in terms of observing the corona forming block in conventional TEM images. Dark field scanning transmission electron microscopy (STEM) was used to characterize the micelle without the negative staining. The micrographs (Figure S23) illustrate the contrast between the core (dark) and the corona (bright). Measurements of core width ($W_{n, core}$) and corona width ($W_{n, corona}$) gave values of 24 and 18 nm, respectively. Based on the core height and width, the cross-section appears to be rectangular or a distorted oval or ellipse, rather than circular.
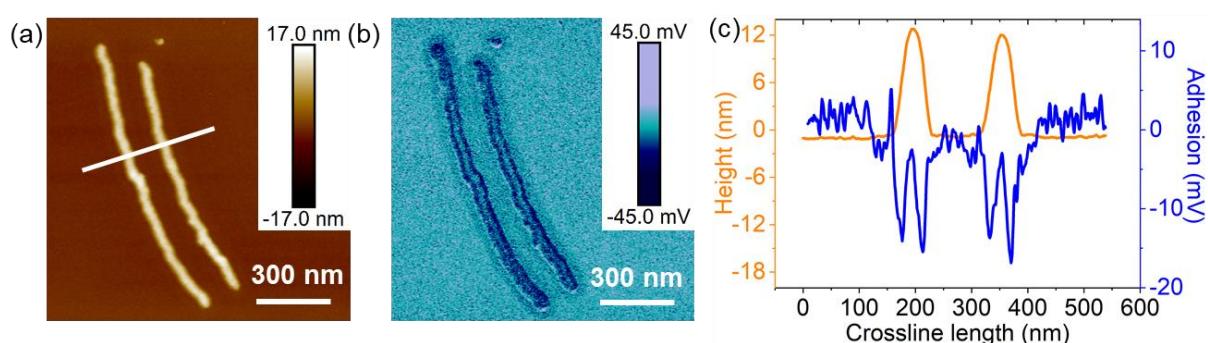
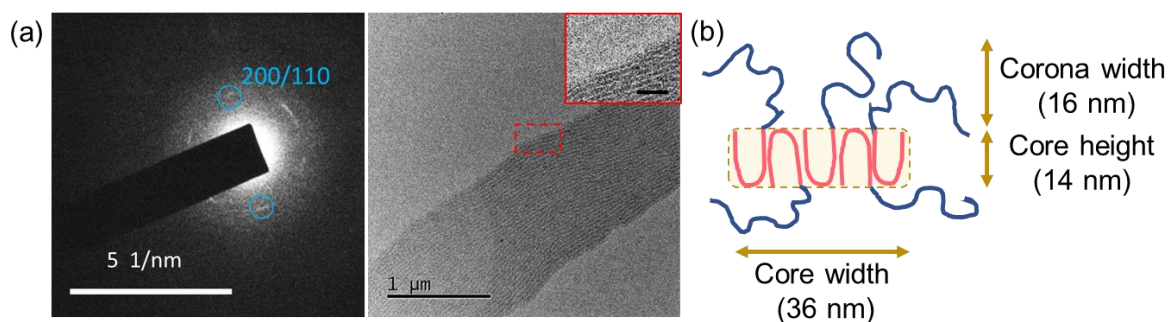**Figure 6.** AFM images of PLLA$_{47}$-b-PNIPAm$_{267}$ micelles with controlled length. (a) Height image of micelles; (b) adhesion image of micelles; (c) linear height (orange) and adhesion (blue) profiles from (a) and (b).

To probe more details on the core structure, powder X-ray diffraction (PXRD) was carried out by drop-casting the micelle solution on a silicon substrate. The results showed weak

broad Bragg peaks at $2\theta = 16.7°$, $19.0°$ and $23.0°$ (Figure S24a). This is in good agreement with the α-form crystalline PLLA.[96] These angles correspond to the crystal planes with Miller indices of (200/110), (203/113) and (213) with d-spacing of 5.37, 4.66 and 3.86 Å, respectively. The weak intensity of these peaks due to the small volume fractions of PLLA in PLLA$_{47}$-b-PNIPAm$_{267}$ BCP. Wide angle X-ray scattering (WAXS) was also employed to confirm crystalline PLLA in the micelle core. A weak Bragg peak at q values of 1.18 Å^{-1} can be observed (Figure S24b). This is consistent with the (200/110) reflections in the crystalline PLLA domains[96].

Selected area electron diffraction (SAED) was also employed to analyze the internal structure of the fiber-like micelles. Due to the rapid destruction of the micelles during irradiation by the electron beam, a video record was taken during the SAED experiment instead of a single image. The SAED image was a screenshot of the video recording when the beam was irradiating the micelles. A *quasi*-hexagonal pattern was obtained by SAED (Figure 7a). The diffraction pattern was shown as short lines (or stretched dots) rather than single dots, which is presumably a consequence of the aggregated and slightly misaligned micelles in the irradiation area on the TEM grid. The d-spacing was calculated as d = 5.43 Å, which is in good agreement with the d-spacing of the (200/110) plane.

From a combination of the PXRD, WAXS and SAED results, the fiber-like micelles have a crystalline PLLA core with the same structure of PLLA α-form single crystal, which has an orthorhombic unit cell consisting of PLLA chains in the form of a 10$_3$ helix with a = 10.7 Å, b = 6.2 Å, and c = 28.8 Å.[97] To explore the orientation of the PLLA chains in the core, the fully extended PLLA chain length was calculated according to the reported PLLA α-form crystal unit cell data. In a PLLA unit cell, a 10$_3$ helix chain has a length of 28.8 nm (which is the length of c), which implies that a single repeat unit has a length of 2.88 nm. In the diblock copolymer PLLA$_{47}$-b-PNIPAm$_{267}$, a fully extended PLLA chain should have a length of 27.5 nm. Based on the AFM data (core width of 36 nm and core height of 14 nm), the PLLA chains appear to fold once and to pack perpendicular to the long axis of the core in the micelle (Figure 7b).

Figure 7. Micelle characterization by SAED. (a) SAED pattern of PLLA$_{47}$-*b*-PNIPAm$_{267}$ micelles; TEM images of micelles in the area for SAED pattern record; aggregated and slight misaligned fiber-like micelles; inset scale bar: 200 nm; (b) Schematic representation of micelle cross-section by AFM characterization. Blue: folded core chains; pink: collapsed corona chains.

To better understand the core structure of the PLLA$_{47}$-*b*-PNIPAm$_{267}$ micelles and to probe the shape of the core cross-section, small-angle X-ray scattering (SAXS) was employed to analyze solutions of PLLA$_{47}$-*b*-PNIPAm$_{267}$. To probe the cross-section of the micelle core, the analysis of SAXS data focused on the sample of 4 mg/mL. This concentration has been found low enough for the scattering intensity (S(Q)) to be regarded as constant.[32, 72]

Two models (Figure S25) were employed to analyze and fit the scattering intensity. Model 1 involved long core-shell rods containing a core of circular cross-section and of homogeneous density and surrounded by a symmetrical shell with a decaying density. This model has been reported to fit the scattering intensity of PFS-*b*-PI cylindrical micelles in solution.[32] Model 2 (Figure S33) describes a long rod-like structure containing a core of homogeneous density with a rectangular cross-section, and decaying density corona attached on the two long core edges. Fitting was conducted with a non-linear least-squares method to allow for the scaling factor, background, core and corona dimensions, scattering-length density (SLD) of corona, and polydispersity of core and corona to refine.

Both the models give good fits for the measured scattering intensity of the sample solutions in the whole experimental *q* range (Figure S26). The error bars on the experimental data are small, especially at high *q* range, which is a result of data grouping during the interpretation process (the bin sizes of the data grouping increase as the q values become larger.) Although the scattering intensity fits well, the scattering intensity residuals from Model 1 scattered randomly away from zero in an unsymmetrical pattern and with a large amplitude (ca. 4, while a good fitting would have an amplitude around 1) (Figure S27). This result suggests that cylindrical rods with a circular cross-section may not provide a perfect fit for the

14

micelles. To better probe the nature of the micelle cross-section, AFM and STEM results were taken into consideration (Table 1). The data from the model 2 fitting agrees well with the AFM measurement except in core height, which may be due to the collapsed corona on the core surface which resulting in height increase. The difference in core width measured by STEM may be caused by the low resolution of core and corona boundary due to the low electron density of PLLA$_{47}$-b-PNIPAm$_{267}$. In general, model 2 with a rectangular cross-section fits well with PLLA$_{47}$-b-PNIPAm$_{267}$ micelles. However, the possibility of elliptical cross-section cannot be excluded.

Table 1. Summary of size characterizations by STEM, AFM and SAXS of PLLA$_{47}$-b-PEG$_{267}$ micelles ($L_n = 1040$ nm, $L_w/L_n = 1.04$) prepared at 4 mg/mL in EtOH.

Technique	Length (nm)	Core height (nm)	Core width (nm)	Corona thickness (nm)
AFM	–	14±0.1*	36	16
STEM	1040±87.2	–	24±4.4	18±3.9
SAXS (Model 1)	–	–	4±0.1	22±0.5
SAXS (Model 2)	–	7±0.7	32±3.6	19±0.9

*Errors represents the measurement standard deviation

8. Extension of the Strategy to PLLA-*b*-P2VP

As a result of the access to efficient living CDSA of PLLA$_{47}$-b-PNIPAm$_{267}$, we attempted to explore the generality of the approach. We therefore transposed a similar approach to PLLA$_{47}$-b-P2VP$_{503}$.

(i) Uniform Fiber-like Micelles via Living CDSA

PLLA$_{47}$-b-P2VP$_{503}$ seed micelles ($L_n = 29$ nm, $L_w/L_n = 1.11$) and seeded-growth experiments were carried out in TFE/EtOH in similar procedures as PLLA$_{47}$-b-PNIPAm$_{267}$ (Figure 28). The measured micelle lengths had L_n from ca. 100 nm to ca. 900 nm with $L_w/L_n \leq 1.05$ (Figure 8e and S29). A linear plot of the measured length verses the unimer-to-seed mass ratio was obtained (Figure 8f) and the length increased along the predicted line, which showed a living epitaxial growth of PLLA$_{47}$-b-P2VP$_{503}$ micelles.
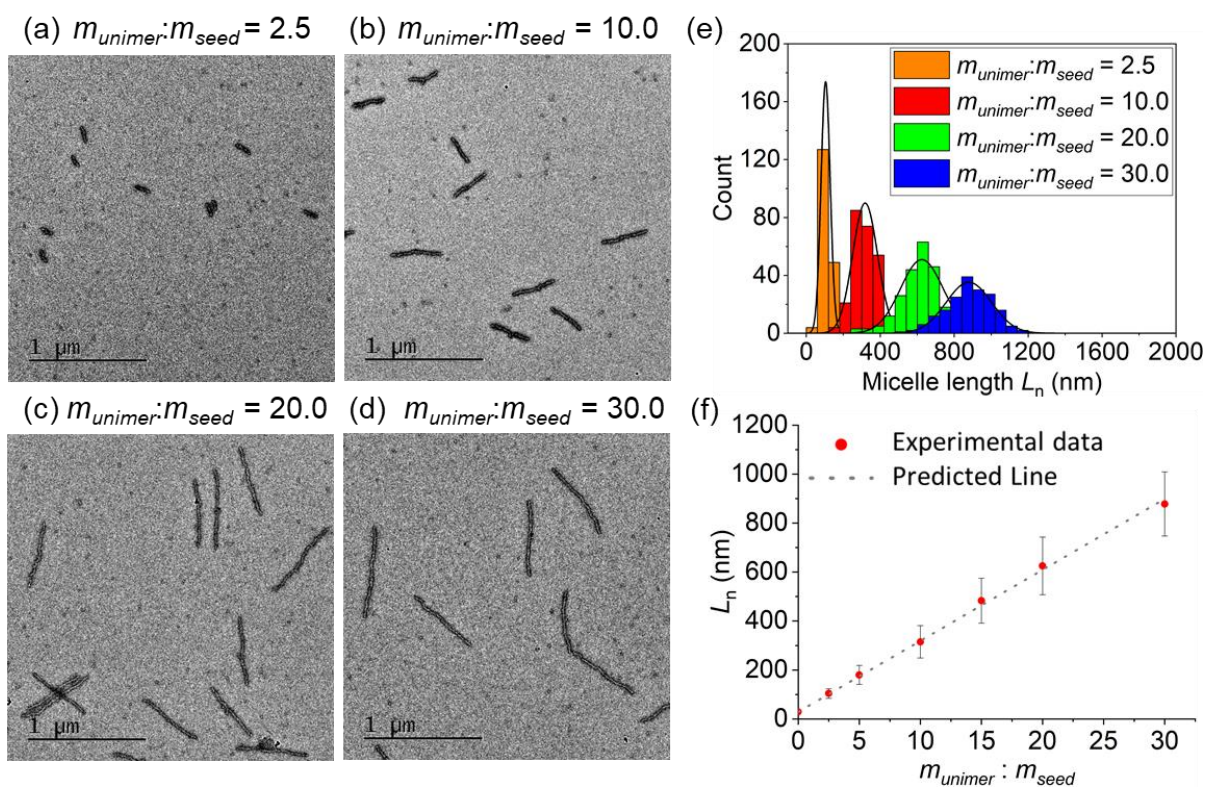
Figure 8. TEM images of samples (aging for 5 days) of uniform PLLA$_{47}$-*b*-P2VP$_{503}$ micelles prepared by seeded growth off seed micelles (L_n = 29 nm, L_w/L_n = 1.11, σ/L_n: 0.34) in TFE/EtOH with volume ratios of (a) 3:97, (b) 5:95, (c) 10:90 and (d) 15:85 after the addition of unimers (in DMSO) with unimer-to-seed mass ratios of (a) 2.5, (b) 10.0, (c) 20.0 and (d) 30.0, respectively; (e) Summary of contour length histograms of micelle length distributions; (f) plot of number average micelle length vs m_{unimer}:m_{seed} (the error bars represent the standard deviation). The predicted length corresponding to a unimer-to-seed mass ratio of 30 is L_n = 899 nm.

Seeded-growth experiments in pure EtOH without TFE were also conducted as control experiments (Figure S30 and S31). The fiber-like micelles obtained had shorter lengths compared with those predicted theoretically. With increasing unimer-to-seed mass ratios, the micelle length dispersity indices were found to increase significantly. These results confirmed that controlled epitaxial growth requires the presence of the TFE cosolvent.

(ii) Preparation of Block Co-micelles

Living CDSA allows the preparation of complex micelle structures such as block co-micelle with well-defined segments of different control chemistry. PLLA-based block co-micelles have not been successfully prepared to date and we attempted to use the improved living CDSA approach to prepare triblock and subsequently pentablock co-micelles from the PLLA$_{47}$-*b*-PNIPAm$_{267}$ and PLLA$_{47}$-*b*-P2VP$_{503}$ diblock copolymers.

16

Two pentablock co-micelles (pentablock 1, L_n = 716 nm; and pentablock 2, L_n = 1131 nm, Figure 9 and S32) with narrow length dispersities were prepared by alternating growth using PLLA$_{47}$-b-P2VP$_{503}$ and PLLA$_{47}$-b-PNIPAm$_{267}$ as unimers from PLLA$_{47}$-b-PNIPAm$_{267}$ and PLLA$_{47}$-b-P2VP$_{503}$ seeds, respectively. The PLLA$_{47}$-b-P2VP$_{503}$ seeds (Figure S28) were prepared analogously to those of PLLA$_{47}$-b-PNIPAm$_{267}$. The prepared triblock and pentablock co-micelles showed clear segmented structures after staining and the different micelle segments is enhanced by the electron contrast between the PNIPAm and P2VP coronas.
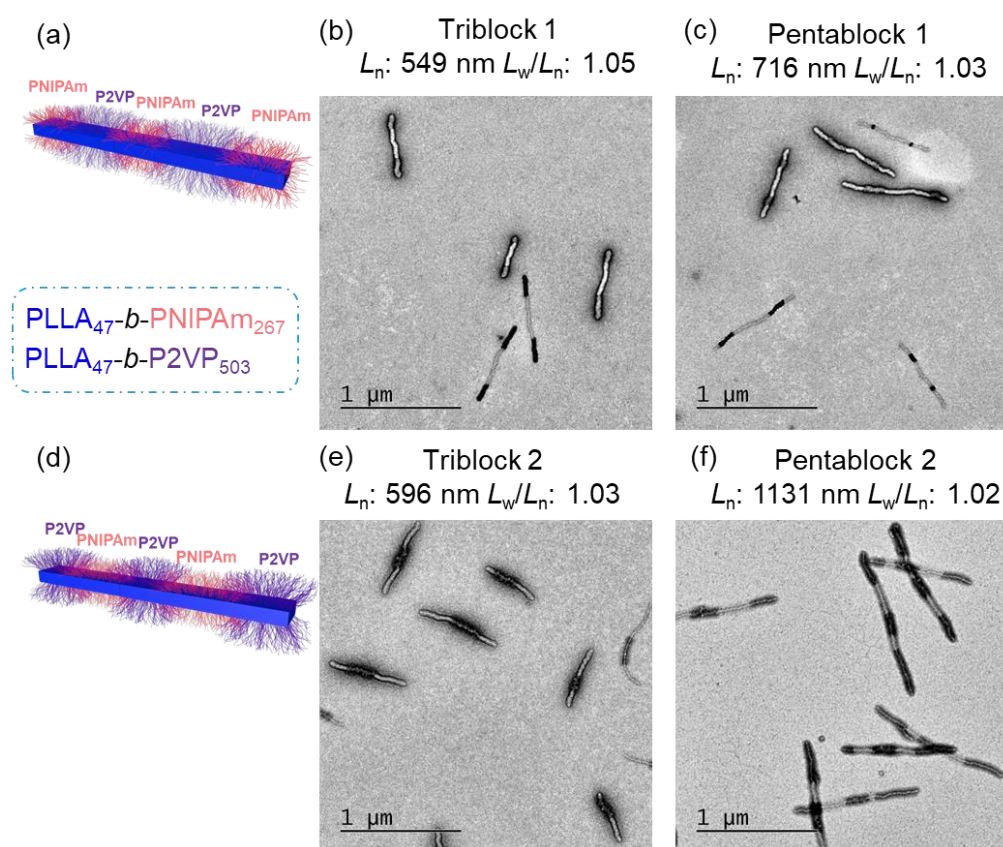
Figure 9. Preparation of pentablock co-micelles with PLLA$_{47}$-b-PNIPAm$_{267}$ and PLLA$_{47}$-b-P2VP$_{503}$ diblock copolymers. (a and d) Representation of two pentablock co-micelles; TEM images of (b) triblock co-micelles 1 (L_n = 549 nm, L_w/L_n = 1.05), (c) pentablock co-micelles 1 (L_n = 716 nm, L_w/L_n = 1.03), (e) triblock co-micelles 2 (L_n = 596 nm, L_w/L_n = 1.03), and (f) pentablock co-micelles 2 (L_n = 1131 nm, L_w/L_n = 1.02),. TEM samples were stained with a 2 wt% solution of uranyl acetate in EtOH.

9. DISCUSSION

Initial seeded-growth experiments with PLLA$_{47}$-b-PNIPAm$_{267}$ in EtOH revealed poor control of fiber length and significant dispersities for the resulting length distributions. Evidence for self-nucleation competing with seeded-growth was provided by the presence of the shoulder

peaks in the low micelle length region in the contour length histograms (Figure S9). The observation of a small but significant quantity of non-spherical nanoparticles on the TEM grids (Figure S8) was consistent with the aggregation of unimers under conditions where the PLLA core has insufficient time to crystallize. This process would deplete the reservoir of unimer available for seeded-growth and, together with self-nucleation, would be expected to lead to fiber-like micelles possessing lower L_n values that those predicted values based on the unimer-to-seed mass ratios. Similar results were also observed for the seeded-growth of PLLA$_{47}$-b-P2VP$_{503}$ in pure EtOH (Figure S30).

In contrast, when TFE was added as a cosolvent to EtOH, seeded-growth of PLLA$_{47}$-b-PNIPAm$_{267}$ afforded uniform fibers with close to predicted lengths up to ca. 1 μm. Further studies indicated that other solvent additives, such as DMF, DMSO and acetone also lead to a substantial increase in the efficiency of the living CDSA growth process. An explanation for the improved efficiency of living CDSA in the presence of these cosolvents appears to most likely to involve disruption of H-bond between PLLA chains which otherwise contributes to undesirable unimer self-nucleation and aggregation. We investigated other possible factors such as changes in solvent polarity and polymer solubility related to dielectric constant and logP$_{oct}$, respectively. In neither case was a convincing correlation found and we therefore postulate that the ability of TFE, DMF, DMSO and acetone to facilitate efficient living CDSA through their ability to function as H-bonding disruptors as the most likely explanation for our observations (Figure 10).
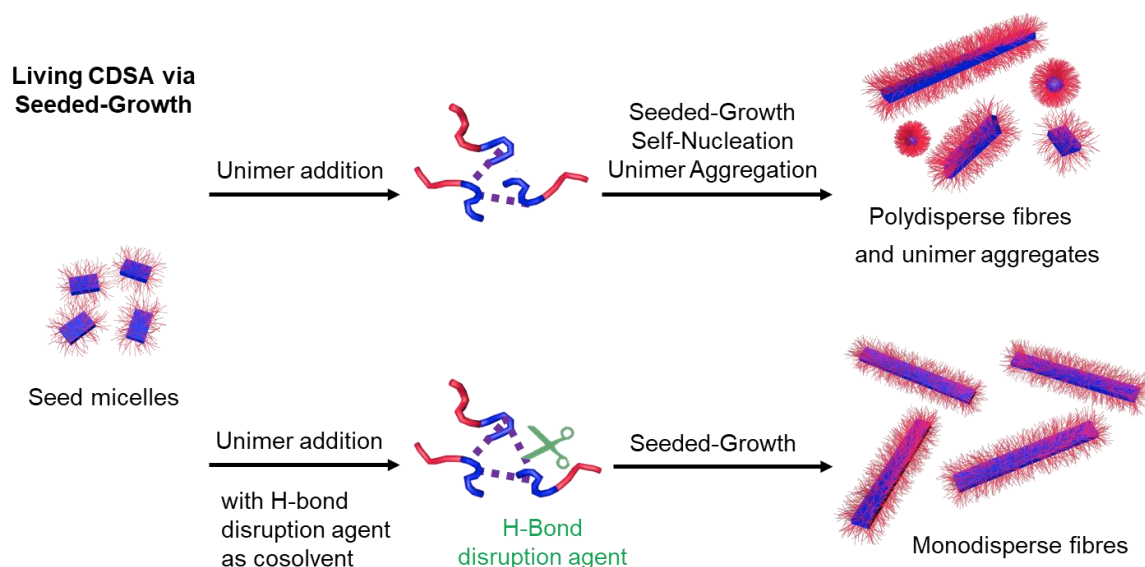
Figure 10. Schematic representation of improvement in the efficiency of seeded-growth of PLLA diblock copolymers using H-bond disruption agents.

SUMMARY

"Living CDSA" seeded growth methods represent a highly promising approach to 1D and 2D core-shell nanoparticles of controllable and uniform size and tailored complexity based on crystallizable polymer amphiphiles. The living CDSA method was initially developed for PFS metalloblock copolymers and the past decade has seen an impressive expansion of the approach to a wide range of crystallizable organic polymers and also π-stacking molecular species. However, in several cases attempts to develop efficient living CDSA approaches have been a substantial challenge and dimensional control has been imperfect. The case of PLLA block copolymers provides an excellent example. In this paper we have demonstrated that the problems arising from self-nucleation and unimer aggregation for PLLA block copolymers can be overcome by variation of the solvent medium. Thus, the addition of TFE, DMF, DMSO and acetone as cosolvents to EtOH as selective solvent leads to impressive improvement in the efficiency of living CDSA allowing the formation of not only uniform fiber-like micelles of controlled length up to over 1 μm but also block comicelles from the diblock copolymers $PLLA_{47}$-b-$PNIPAm_{267}$ and $PLLA_{47}$-b-$P2VP_{503}$. We attribute the improved efficiency to the ability of the cosolvents to act as H-bond disruptors which reduces undesirable interactions between the PLLA segments in the unimers and the consequential self-nucleation. Our results suggest that the use of analogous approaches to achieve improved solvency may be effective for other systems where the living CDSA behavior has been inefficient to date.

As part of our studies we have also provided detailed characterization of $PLLA_{47}$-b-$PNIPAm_{267}$ fiber-like micelles by AFM, SAED and SAXS. The results showed that the 1D micelles possess a crystalline chain-folded PLLA core (α-form) with a rectangular or elliptical cross-section single crystal surrounded by solvent swollen PNIPAm corona.

ASSOCIATED CONTENT

Supporting Information

The Supporting Information is available free of charge on the ACS Publications website at DOI: xxxx. Experimental details and additional results (PDF)

AUTHOR INFORMATION

Corresponding Author
*E-mail: a.dove@bham.ac.uk

r.oreilly@bham.ac.uk

imanners@uvic.ca

ORCID

Yunxiang He: 0000-0001-5275-2691

Jean-Charles Eloi: 0000-0003-3487-3996

Robert L. Harniman: 0000-0002-3452-1213

George R. Whittell: 0000-0001-8559-0166

Robert T. Mathers: 0000-0002-0503-4571

Rachel K. O'Reilly: 0000-0002-1043-7172

Andrew P. Dove: 0000-0001-8208-9309

Ian Manners: 0000-0002-3794-967X

Author Contributions

The authors declare no competing financial interest.

Acknowledgment

References

1.   Mai, Y.; Eisenberg, A., Self-assembly of block copolymers. *Chem Soc Rev* **2012,** *41* (18), 5969-85.

2.   Fang, B.; Walther, A.; Wolf, A.; Xu, Y.; Yuan, J.; Muller, A. H., Undulated multicompartment cylinders by the controlled and directed stacking of polymer micelles with a compartmentalized corona. *Angew Chem Int Ed Engl* **2009,** *48* (16), 2877-80.

3.   Ladmiral, V.; Semsarilar, M.; Canton, I.; Armes, S. P., Polymerization-induced self-assembly of galactose-functionalized biocompatible diblock copolymers for intracellular delivery. *J Am Chem Soc* **2013,** *135* (36), 13574-81.

4.   Ge, Z.; Liu, S., Functional block copolymer assemblies responsive to tumor and intracellular microenvironments for site-specific drug delivery and enhanced imaging performance. *Chem Soc Rev* **2013,** *42* (17), 7289-325.

5.   Geng, Y.; Dalhaimer, P.; Cai, S.; Tsai, R.; Tewari, M.; Minko, T.; Discher, D. E., Shape effects of filaments versus spherical particles in flow and drug delivery. *Nat Nanotechnol* **2007,** *2* (4), 249-55.

6.   Gratton, S. E.; Ropp, P. A.; Pohlhaus, P. D.; Luft, J. C.; Madden, V. J.; Napier, M. E.; DeSimone, J. M., The effect of particle design on cellular internalization pathways. *Proc Natl Acad Sci U S A* **2008,** *105* (33), 11613-8.

7.   Albanese, A.; Tang, P. S.; Chan, W. C., The effect of nanoparticle size, shape, and surface chemistry on biological systems. *Annu Rev Biomed Eng* **2012,** *14*, 1-16.

8.   Zhang, K.; Rossin, R.; Hagooly, A.; Chen, Z.; Welch, M. J.; Wooley, K. L., Folate-mediated Cell Uptake of Shell-crosslinked Spheres and Cylinders. *J Polym Sci A Polym Chem* **2008,** *46* (22), 7578-7583.

9.   Khandpur, A. K.; Foerster, S.; Bates, F. S.; Hamley, I. W.; Ryan, A. J.; Bras, W.; Almdal, K.; Mortensen, K., Polyisoprene-Polystyrene Diblock Copolymer Phase Diagram near the Order-Disorder Transition. *Macromolecules* **1995,** *28* (26), 8796-8806.

10.   Foster, J. C.; Varlas, S.; Couturaud, B.; Coe, Z.; O'Reilly, R. K., Getting into Shape: Reflections on a New Generation of Cylindrical Nanostructures' Self-Assembly Using Polymer Building Blocks. *J Am Chem Soc* **2019,** *141* (7), 2742-2753.

11.   Tritschler, U.; Pearce, S.; Gwyther, J.; Whittell, G. R.; Manners, I., 50th Anniversary Perspective: Functional Nanoparticles from the Solution Self-Assembly of Block Copolymers. *Macromolecules* **2017,** *50* (9), 3439-3463.

12.   Zhang, L.; Eisenberg, A., Multiple Morphologies of "Crew-Cut" Aggregates of Polystyrene-b-poly(acrylic acid) Block Copolymers. *Science* **1995,** *268* (5218), 1728-31.

13.   Won, Y. Y.; Davis, H. T.; Bates, F. S., Giant Wormlike Rubber Micelles. *Science* **1999,** *283* (5404), 960-963.

14.   Grumelard, J.; Taubert, A.; Meier, W., Soft nanotubes from amphiphilic ABA triblock macromonomers. *Chem Commun (Camb)* **2004,** (13), 1462-3.

15.   Hamley, I. W., Nanoshells and nanotubes from block copolymers. *Soft Matter* **2005,** *1* (1).

16.   Cheng, C.; Qi, K.; Germack, D. S.; Khoshdel, E.; Wooley, K. L., Synthesis of Core-Crosslinked Nanoparticles with Controlled Cylindrical Shape and Narrowly-Dispersed Size via Core-Shell Brush Block Copolymer Templates. *Advanced Materials* **2007,** *19* (19), 2830-2835.

17.   Dreiss, C. c. A., Wormlike micelles: where do we stand? Recent developments, linear rheology and scattering techniques. *Soft Matter* **2007,** *3* (8).

18.   Huang, K.; Canterbury, D. P.; Rzayev, J., Synthesis of Segmented Polylactide Molecular Brushes and Their Transformation to Open-End Nanotubes. *Macromolecules* **2010,** *43* (16), 6632-6638.

19.   He, W.-N.; Xu, J.-T., Crystallization assisted self-assembly of semicrystalline block copolymers. *Progress in Polymer Science* **2012,** *37* (10), 1350-1400.

20.   Wang, X.; Guerin, G.; Wang, H.; Wang, Y.; Manners, I.; Winnik, M. A., Cylindrical block copolymer micelles and co-micelles of controlled length and architecture. *Science* **2007,** *317* (5838), 644-7.

21.   Gilroy, J. B.; Gadt, T.; Whittell, G. R.; Chabanne, L.; Mitchels, J. M.; Richardson, R. M.; Winnik, M. A.; Manners, I., Monodisperse cylindrical micelles by crystallization-driven living self-assembly. *Nat Chem* **2010,** *2* (7), 566-70.

22.   Qiu, H.; Gao, Y.; Du, V. A.; Harniman, R.; Winnik, M. A.; Manners, I., Branched micelles by living crystallization-driven block copolymer self-assembly under kinetic control. *J Am Chem Soc* **2015,** *137* (6), 2375-85.

23.   Hailes, R. L.; Oliver, A. M.; Gwyther, J.; Whittell, G. R.; Manners, I., Polyferrocenylsilanes: synthesis, properties, and applications. *Chem Soc Rev* **2016,** *45* (19), 5358-407.

24.   Cao, L.; Manners, I.; Winnik, M. A., Influence of the Interplay of Crystallization and Chain Stretching on Micellar Morphologies: Solution Self-Assembly of Coil–Crystalline Poly(isoprene-block-ferrocenylsilane). *Macromolecules* **2002,** *35* (22), 8258-8260.

25.   Rupar, P. A.; Chabanne, L.; Winnik, M. A.; Manners, I., Non-centrosymmetric cylindrical micelles by unidirectional growth. *Science* **2012,** *337* (6094), 559-62.

26.   Hudson, Z. M.; Lunn, D. J.; Winnik, M. A.; Manners, I., Colour-tunable fluorescent multiblock micelles. *Nat Commun* **2014,** *5*, 3372.

27.   Wang, X.; Liu, K.; Arsenault, A. C.; Rider, D. A.; Ozin, G. A.; Winnik, M. A.; Manners, I., Shell-cross-linked cylindrical Polyisoprene-b-polyferrocenylsilane (PI-b-PFS) block copolymer micelles: one-dimensional (1D) organometallic nanocylinders. *J Am Chem Soc* **2007,** *129* (17), 5630-9.

28.   Qiu, H.; Hudson, Z. M.; Winnik, M. A.; Manners, I., Micelle assembly. Multidimensional hierarchical self-assembly of amphiphilic cylindrical block comicelles. *Science* **2015,** *347* (6228), 1329-32.

29.   Mohd Yusoff, S. F.; Hsiao, M.-S.; Schacher, F. H.; Winnik, M. A.; Manners, I., Formation of Lenticular Platelet Micelles via the Interplay of Crystallization and Chain Stretching: Solution Self-Assembly of Poly(ferrocenyldimethylsilane)-block-poly(2-vinylpyridine) with a Crystallizable Core-Forming Metalloblock. *Macromolecules* **2012,** *45* (9), 3883-3891.

30.   Qiu, H.; Gao, Y.; Boott, C. E.; Gould, O. E.; Harniman, R. L.; Miles, M. J.; Webb, S. E.; Winnik, M. A.; Manners, I., Uniform patchy and hollow rectangular platelet micelles from crystallizable polymer blends. *Science* **2016,** *352* (6286), 697-701.

31.   He, X.; Hsiao, M. S.; Boott, C. E.; Harniman, R. L.; Nazemi, A.; Li, X.; Winnik, M. A.; Manners, I., Two-dimensional assemblies from crystallizable homopolymers with charged termini. *Nat Mater* **2017,** *16* (4), 481-488.

32.   Hayward, D. W.; Gilroy, J. B.; Rupar, P. A.; Chabanne, L.; Pizzey, C.; Winnik, M. A.; Whittell, G. R.; Manners, I.; Richardson, R. M., Liquid Crystalline Phase Behavior of Well-Defined Cylindrical Block Copolymer Micelles Using Synchrotron Small-Angle X-ray Scattering. *Macromolecules* **2015,** *48* (5), 1579-1591.

33.   Gould, O. E.; Qiu, H.; Lunn, D. J.; Rowden, J.; Harniman, R. L.; Hudson, Z. M.; Winnik, M. A.; Miles, M. J.; Manners, I., Transformation and patterning of supermicelles using dynamic holographic assembly. *Nat Commun* **2015,** *6*, 10009.

34.   Nazemi, A.; Boott, C. E.; Lunn, D. J.; Gwyther, J.; Hayward, D. W.; Richardson, R. M.; Winnik, M. A.; Manners, I., Monodisperse Cylindrical Micelles and Block Comicelles of Controlled Length in Aqueous Media. *J Am Chem Soc* **2016,** *138* (13), 4484-93.

35.   Dou, H.; Li, M.; Qiao, Y.; Harniman, R.; Li, X.; Boott, C. E.; Mann, S.; Manners, I., Higher-order assembly of crystalline cylindrical micelles into membrane-extendable colloidosomes. *Nat Commun* **2017,** *8* (1), 426.

36.   Schmalz, H.; Schmelz, J.; Drechsler, M.; Yuan, J.; Walther, A.; Schweimer, K.; Mihut, A. M., Thermo-Reversible Formation of Wormlike Micelles with a Microphase-Separated Corona from a Semicrystalline Triblock Terpolymer. *Macromolecules* **2008,** *41* (9), 3235-3242.

37.   Schmelz, J.; Schedl, A. E.; Steinlein, C.; Manners, I.; Schmalz, H., Length control and block-type architectures in worm-like micelles with polyethylene cores. *J Am Chem Soc* **2012,** *134* (34), 14217-25.

38.   Yin, L.; Lodge, T. P.; Hillmyer, M. A., A Stepwise "Micellization–Crystallization" Route to Oblate Ellipsoidal, Cylindrical, and Bilayer Micelles with Polyethylene Cores in Water. *Macromolecules* **2012,** *45* (23), 9460-9467.

39.   Schöbel, J.; Karg, M.; Rosenbach, D.; Krauss, G.; Greiner, A.; Schmalz, H., Patchy Wormlike Micelles with Tailored Functionality by Crystallization-Driven Self-Assembly: A Versatile Platform for Mesostructured Hybrid Materials. *Macromolecules* **2016,** *49* (7), 2761-2771.

40.   Patra, S. K.; Ahmed, R.; Whittell, G. R.; Lunn, D. J.; Dunphy, E. L.; Winnik, M. A.; Manners, I., Cylindrical micelles of controlled length with a pi-conjugated polythiophene core via crystallization-driven self-assembly. *J Am Chem Soc* **2011,** *133* (23), 8842-5.

41.   Gwyther, J.; Gilroy, J. B.; Rupar, P. A.; Lunn, D. J.; Kynaston, E.; Patra, S. K.; Whittell, G. R.; Winnik, M. A.; Manners, I., Dimensional control of block copolymer nanofibers with a pi-conjugated core: crystallization-driven solution self-assembly of amphiphilic poly(3-hexylthiophene)-b-poly(2-vinylpyridine). *Chemistry* **2013,** *19* (28), 9186-97.

42.   Qian, J.; Li, X.; Lunn, D. J.; Gwyther, J.; Hudson, Z. M.; Kynaston, E.; Rupar, P. A.; Winnik, M. A.; Manners, I., Uniform, high aspect ratio fiber-like micelles and block co-micelles with a crystalline pi-conjugated polythiophene core by self-seeding. *J Am Chem Soc* **2014,** *136* (11), 4121-4.

43.   Kamps, A. C.; Fryd, M.; Park, S. J., Hierarchical self-assembly of amphiphilic semiconducting polymers into isolated, bundled, and branched nanofibers. *ACS Nano* **2012,** *6* (3), 2844-52.

44.   Lee, I. H.; Amaladass, P.; Yoon, K. Y.; Shin, S.; Kim, Y. J.; Kim, I.; Lee, E.; Choi, T. L., Nanostar and nanonetwork crystals fabricated by in situ nanoparticlization of fully conjugated polythiophene diblock copolymers. *J Am Chem Soc* **2013,** *135* (47), 17695-8.

45.   Kynaston, E. L.; Nazemi, A.; MacFarlane, L. R.; Whittell, G. R.; Faul, C. F. J.; Manners, I., Uniform Polyselenophene Block Copolymer Fiberlike Micelles and Block Co-micelles via Living Crystallization-Driven Self-Assembly. *Macromolecules* **2018,** *51* (3), 1002-1010.

46.   Tung, Y.-C.; Wu, W.-C.; Chen, W.-C., Morphological Transformation and Photophysical Properties of Rod-Coil Poly[2,7-(9,9-dihexylfluorene)]-block-poly(acrylic acid) in Solution. *Macromolecular Rapid Communications* **2006,** *27* (21), 1838-1844.

47.   Tian, Y.; Chen, C.-Y.; Yip, H.-L.; Wu, W.-C.; Chen, W.-C.; Jen, A. K. Y., Synthesis, Nanostructure, Functionality, and Application of Polyfluorene-block-poly(N-isopropylacrylamide)s. *Macromolecules* **2010,** *43* (1), 282-291.

48.   Li, K.; Wang, Q., Multiple self-assembled nanostructures from an oligo(p-phenyleneethynylene) containing rod-coil-rod triblock copolymer. *Chem Commun (Camb)* **2005,** (38), 4786-8.

49.   Leclère, P.; Calderone, A.; Marsitzky, D.; Francke, V.; Geerts, Y.; Müllen, K.; Brédas, J. L.; Lazzaroni, R., Highly Regular Organization of Conjugated Polymer Chains via Block Copolymer Self-Assembly. *Advanced Materials* **2000,** *12* (14), 1042-1046.

50.   Wang, H.; Wang, H. H.; Urban, V. S.; Littrell, K. C.; Thiyagarajan, P.; Yu, L., Syntheses of Amphiphilic Diblock Copolymers Containing a Conjugated Block and Their Self-Assembling Properties. *Journal of the American Chemical Society* **2000,** *122* (29), 6855-6861.

51.   Han, L.; Wang, M.; Jia, X.; Chen, W.; Qian, H.; He, F., Uniform two-dimensional square assemblies from conjugated block copolymers driven by pi-pi interactions with controllable sizes. *Nat Commun* **2018,** *9* (1), 865.

52.   Jin, X. H.; Price, M. B.; Finnegan, J. R.; Boott, C. E.; Richter, J. M.; Rao, A.; Menke, S. M.; Friend, R. H.; Whittell, G. R.; Manners, I., Long-range exciton transport in conjugated polymer nanofibers prepared by seeded growth. *Science* **2018,** *360* (6391), 897-900.

53.   Shin, S.; Menk, F.; Kim, Y.; Lim, J.; Char, K.; Zentel, R.; Choi, T. L., Living Light-Induced Crystallization-Driven Self-Assembly for Rapid Preparation of Semiconducting Nanofibers. *J Am Chem Soc* **2018,** *140* (19), 6088-6094.

54.   Brannigan, R. P.; Dove, A. P., Synthesis, properties and biomedical applications of hydrolytically degradable materials based on aliphatic polyesters and polycarbonates. *Biomater Sci* **2016,** *5* (1), 9-21.

55.   Vroman, I.; Tighzert, L., Biodegradable Polymers. *Materials* **2009,** *2* (2), 307-344.

56.   Petzetakis, N.; Dove, A. P.; O'Reilly, R. K., Cylindrical micelles from the living crystallization-driven self-assembly of poly(lactide)-containing block copolymers. *Chem. Sci.* **2011,** *2* (5), 955-960.

57.   Petzetakis, N.; Walker, D.; Dove, A. P.; O'Reilly, R. K., Crystallization-driven sphere-to-rod transition of poly(lactide)-b-poly(acrylic acid) diblock copolymers: mechanism and kinetics. *Soft Matter* **2012,** *8* (28).

58.   Sun, L.; Petzetakis, N.; Pitto-Barry, A.; Schiller, T. L.; Kirby, N.; Keddie, D. J.; Boyd, B. J.; O'Reilly, R. K.; Dove, A. P., Tuning the Size of Cylindrical Micelles from Poly(l-lactide)-b-poly(acrylic acid) Diblock Copolymers Based on Crystallization-Driven Self-Assembly. *Macromolecules* **2013,** *46* (22), 9074-9082.

59.   Fu, J.; Luan, B.; Yu, X.; Cong, Y.; Li, J.; Pan, C.; Han, Y.; Yang, Y.; Li, B., Self-Assembly of Crystalline–Coil Diblock Copolymer in Solvents with Varying Selectivity: From Spinodal-like Aggregates to Spheres, Cylinders, and Lamellae. *Macromolecules* **2004,** *37* (3), 976-986.

60.   He, W.-N.; Zhou, B.; Xu, J.-T.; Du, B.-Y.; Fan, Z.-Q., Two Growth Modes of Semicrystalline Cylindrical Poly(ε-caprolactone)-b-poly(ethylene oxide) Micelles. *Macromolecules* **2012,** *45* (24), 9768-9778.

61.   Du, Z.-X.; Xu, J.-T.; Fan, Z.-Q., Micellar Morphologies of Poly(ε-caprolactone)-b-poly(ethylene oxide) Block Copolymers in Water with a Crystalline Core. *Macromolecules* **2007,** *40* (21), 7633-7637.

62.   Du, Z.-X.; Xu, J.-T.; Fan, Z.-Q., Regulation of Micellar Morphology of PCL-b-PEO Block Copolymers by Crystallization Temperature. *Macromolecular Rapid Communications* **2008,** *29* (6), 467-471.

63.   Sun, L.; Pitto-Barry, A.; Kirby, N.; Schiller, T. L.; Sanchez, A. M.; Dyson, M. A.; Sloan, J.; Wilson, N. R.; O'Reilly, R. K.; Dove, A. P., Structural reorganization of cylindrical nanoparticles triggered by polylactide stereocomplexation. *Nat Commun* **2014,** *5*, 5746.

64.   Inam, M.; Cambridge, G.; Pitto-Barry, A.; Laker, Z. P. L.; Wilson, N. R.; Mathers, R. T.; Dove, A. P.; O'Reilly, R. K., 1D vs. 2D shape selectivity in the crystallization-driven self-assembly of polylactide block copolymers. *Chem Sci* **2017,** *8* (6), 4223-4230.

65.   Yu, W.; Inam, M.; Jones, J. R.; Dove, A. P.; O'Reilly, R. K., Understanding the CDSA of poly(lactide) containing triblock copolymers. *Polymer Chemistry* **2017,** *8* (36), 5504-5512.

66.   Wang, J.; Zhu, W.; Peng, B.; Chen, Y., A facile way to prepare crystalline platelets of block copolymers by crystallization-driven self-assembly. *Polymer* **2013,** *54* (25), 6760-6767.

67.   Zhang, J.; Wang, L. Q.; Wang, H.; Tu, K., Micellization phenomena of amphiphilic block copolymers based on methoxy poly(ethylene glycol) and either crystalline or amorphous poly(caprolactone-b-lactide). *Biomacromolecules* **2006,** *7* (9), 2492-500.

68.   Rizis, G.; van de Ven, T. G.; Eisenberg, A., Crystallinity-driven morphological ripening processes for poly(ethylene oxide)-block-polycaprolactone micelles in water. *Soft Matter* **2014,** *10* (16), 2825-35.

69.   Ganda, S.; Dulle, M.; Drechsler, M.; Förster, B.; Förster, S.; Stenzel, M. H., Two-Dimensional Self-Assembled Structures of Highly Ordered Bioactive Crystalline-Based Block Copolymers. *Macromolecules* **2017,** *50* (21), 8544-8553.

70.   Li, Z.; Zhang, Y.; Wu, L.; Yu, W.; Wilks, T. R.; Dove, A. P.; Ding, H.-m.; O'Reilly, R. K.; Chen, G.; Jiang, M., Glyco-Platelets with Controlled Morphologies via Crystallization-Driven Self-Assembly and Their Shape-Dependent Interplay with Macrophages. *ACS Macro Letters* **2019**, 596-602.

71.   Arno, M. C.; Inam, M.; Coe, Z.; Cambridge, G.; Macdougall, L. J.; Keogh, R.; Dove, A. P.; O'Reilly, R. K., Precision Epitaxy for Aqueous 1D and 2D Poly(epsilon-caprolactone) Assemblies. *J Am Chem Soc* **2017,** *139* (46), 16980-16985.

72.   Finnegan, J. R.; He, X.; Street, S. T. G.; Garcia-Hernandez, J. D.; Hayward, D. W.; Harniman, R. L.; Richardson, R. M.; Whittell, G. R.; Manners, I., Extending the Scope of "Living" Crystallization-

Driven Self-Assembly: Well-Defined 1D Micelles and Block Comicelles from Crystallizable Polycarbonate Block Copolymers. *J Am Chem Soc* **2018,** *140* (49), 17127-17140.

73.   Song, Y.; Chen, Y.; Su, L.; Li, R.; Letteri, R. A.; Wooley, K. L., Crystallization-driven assembly of fully degradable, natural product-based poly(l-lactide)-block-poly(α-d-glucose carbonate)s in aqueous solution. *Polymer* **2017,** *122*, 270-279.

74.   Inam, M.; Jones, J. R.; Perez-Madrigal, M. M.; Arno, M. C.; Dove, A. P.; O'Reilly, R. K., Controlling the Size of Two-Dimensional Polymer Platelets for Water-in-Water Emulsifiers. *ACS Cent Sci* **2018,** *4* (1), 63-70.

75.   He, X.; He, Y.; Hsiao, M. S.; Harniman, R. L.; Pearce, S.; Winnik, M. A.; Manners, I., Complex and Hierarchical 2D Assemblies via Crystallization-Driven Self-Assembly of Poly(l-lactide) Homopolymers with Charged Termini. *J Am Chem Soc* **2017,** *139* (27), 9221-9228.

76.   Qiu, H.; Du, V. A.; Winnik, M. A.; Manners, I., Branched cylindrical micelles via crystallization-driven self-assembly. *J Am Chem Soc* **2013,** *135* (47), 17739-42.

77.   Wasanasuk, K.; Tashiro, K.; Hanesaka, M.; Ohhara, T.; Kurihara, K.; Kuroki, R.; Tamada, T.; Ozeki, T.; Kanamoto, T., Crystal Structure Analysis of Poly(l-lactic Acid) α Form On the basis of the 2-Dimensional Wide-Angle Synchrotron X-ray and Neutron Diffraction Measurements. *Macromolecules* **2011,** *44* (16), 6441-6452.

78.   Kollman, P.; McKelvey, J.; Johansson, A.; Rothenberg, S., Theoretical studies of hydrogen-bonded dimers. Complexes involving HF, H2O, NH3, CH1, H2S, PH3, HCN, HNC, HCP, CH2NH, H2CS, H2CO, CH4, CF3,H, C2H2, C2H4, C6H6, F- and H3O+. *Journal of the American Chemical Society* **1975,** *97* (5), 955-965.

79.   Seiler, P.; Weisman, G. R.; Glendening, E. D.; Weinhold, F.; Johnson, V. B.; Dunitz, J. D., Observation of an Eclipsed Csp3-CH3 Bond in a Tricyclic Orthoamide; Experimental and Theoretical Evidence for C⬚H··O Hydrogen Bonds. *Angewandte Chemie International Edition in English* **1987,** *26* (11), 1175-1177.

80.   Allerhand, A.; Von Rague Schleyer, P., A Survey of C-H Groups as Proton Donors in Hydrogen Bonding. *Journal of the American Chemical Society* **1963,** *85* (12), 1715-1723.

81.   Desiraju, G. R.; Steiner, T., *The weak hydrogen bond : in structural chemistry and biology*. Oxford University Press: Oxford ; New York, 1999; p xiv, 507 p.

82.   Jeffrey, G. A.; Maluszynska, H., A survey of hydrogen bond geometries in the crystal structures of amino acids. *International Journal of Biological Macromolecules* **1982,** *4* (3), 173-185.

83.   Sussman, J. L.; Seeman, N. C.; Kim, S. H.; Berman, H. M., Crystal structure of a naturally occurring dinucleoside phosphate: Uridylyl 3′,5′-adenosine phosphate model for RNA chain folding. *Journal of Molecular Biology* **1972,** *66* (3), 403-421.

84.   Steiner, T.; Saenger, W., Geometry of carbon-hydrogen.cntdot..cntdot..cntdot.oxygen hydrogen bonds in carbohydrate crystal structures. Analysis of neutron diffraction data. *Journal of the American Chemical Society* **1992,** *114* (26), 10146-10154.

85.   Bella, J.; Berman, H. M., Crystallographic evidence for C alpha-H...O=C hydrogen bonds in a collagen triple helix. *J Mol Biol* **1996,** *264* (4), 734-42.

86.   Starzyk, A.; Barber-Armstrong, W.; Sridharan, M.; Decatur, S. M., Spectroscopic evidence for backbone desolvation of helical peptides by 2,2,2-trifluoroethanol: an isotope-edited FTIR study. *Biochemistry* **2005,** *44* (1), 369-76.

87.   Boott, C. E.; Leitao, E. M.; Hayward, D. W.; Laine, R. F.; Mahou, P.; Guerin, G.; Winnik, M. A.; Richardson, R. M.; Kaminski, C. F.; Whittell, G. R.; Manners, I., Probing the Growth Kinetics for the Formation of Uniform 1D Block Copolymer Nanoparticles by Living Crystallization-Driven Self-Assembly. *ACS Nano* **2018,** *12* (9), 8920-8933.

88.   Harwood, L. M.; Moody, C. J.; Percy, J. M., *Experimental organic chemistry : standard and microscale*. 2nd ed.; Blackwell Science: Oxford, 1999; p x, 716 p.

89.   Marcus, Y., Recommended Methods for the Purification of Solvents and Tests for Impurities - 1,2-Ethanediol and 2,2,2-Trifluoroethanol. *Pure and Applied Chemistry* **1990,** *62* (1), 139-147.

90.   Llinas, M.; Klein, M. P., Solution Conformation of Ferrichromes .6. Charge Relay at Peptide-Bond - Proton Magnetic-Resonance Study of Solvation Effects on Amide Electron-Density Distribution. *Journal of the American Chemical Society* **1975,** *97* (16), 4731-4737.

91.   Yildirim, E.; Dakshinamoorthy, D.; Peretic, M. J.; Pasquinelli, M. A.; Mathers, R. T., Synthetic Design of Polyester Electrolytes Guided by Hydrophobicity Calculations. *Macromolecules* **2016,** *49* (20), 7868-7876.

92.   Marcus, Y., The effectiveness of solvents as hydrogen bond donors. *Journal of Solution Chemistry* **1991,** *20* (9), 929-944.

93.   Kamlet, M. J.; Abboud, J. L. M.; Abraham, M. H.; Taft, R. W., Linear solvation energy relationships. 23. A comprehensive collection of the solvatochromic parameters, .pi.*, .alpha., and .beta., and some methods for simplifying the generalized solvatochromic equation. *The Journal of Organic Chemistry* **1983,** *48* (17), 2877-2887.

94.   Hsiao, M.-S.; Yusoff, S. F. M.; Winnik, M. A.; Manners, I., Crystallization-Driven Self-Assembly of Block Copolymers with a Short Crystallizable Core-Forming Segment: Controlling Micelle Morphology through the Influence of Molar Mass and Solvent Selectivity. *Macromolecules* **2014,** *47* (7), 2361-2372.

95.   Gilroy, J. B.; Rupar, P. A.; Whittell, G. R.; Chabanne, L.; Terrill, N. J.; Winnik, M. A.; Manners, I.; Richardson, R. M., Probing the structure of the crystalline core of field-aligned, monodisperse, cylindrical polyisoprene-block-polyferrocenylsilane micelles in solution using synchrotron small- and wide-angle X-ray scattering. *J Am Chem Soc* **2011,** *133* (42), 17056-62.

96.   Li, J.; Xiao, P.; Li, H.; Zhang, Y.; Xue, F.; Luo, B.; Huang, S.; Shang, Y.; Wen, H.; de Claville Christiansen, J.; Yu, D.; Jiang, S., Crystalline structures and crystallization behaviors of poly(l-lactide) in poly(l-lactide)/graphene nanosheet composites. *Polymer Chemistry* **2015,** *6* (21), 3988-4002.

97.   Sasaki, S.; Asakura, T., Helix Distortion and Crystal Structure of the α-Form of Poly(l-lactide). *Macromolecules* **2003,** *36* (22), 8385-8390.

TOC

PLLA diblock copolymer